

Network Structure Control of Binary Mixed Langmuir Monolayers of Homo-PS and PS-*b*-P2VP

Gangyao Wen*

Department of Polymer Materials and Engineering, College of Materials Science and Engineering, Harbin University of Science and Technology, Harbin 150040, P. R. China

Received: October 7, 2009; Revised Manuscript Received: December 22, 2009

Our recent work showed there existed a composition window for mixed Langmuir monolayers of homopolystyrene (h-PS) and a symmetric diblock copolymer polystyrene-*block*-poly(2-vinylpyridine) (PS-*b*-P2VP) to form necklace-network structures at the air/water interface. In order to study further the possible mechanism and control the network structure (i.e., surface coverage and nanoaggregate diameter), effects of spreading solution concentration and volume, subphase temperature, and transfer pressure on the network structure were studied by the Langmuir monolayer technique and tapping mode atomic force microscopy. With the increase of transfer pressure, there existed a novel nonlinear behavior for the nanoaggregate diameter first to increase, then to decrease, and finally to increase again, while the surface coverage tended to increase step by step. Moreover, with the elevation of temperature, chain motion between the adjoining nanoaggregates tended to be improved and thus the nanoaggregate diameter tended to be more uniform.

Introduction

It is well-known that the Langmuir–Blodgett (LB) technique has been used to prepare ultrathin films with well-defined structures.^{1–3} Mechanical, chemical, and thermal stabilities of the polymeric LB films with nanostructures have been improved compared with those of the conventional low-molecular-weight amphiphilic LB films.⁴ Due to the ability to self-assemble into a variety of ordered microstructures, amphiphilic block copolymers have been widely used to prepare the LB films in recent years.^{5–21} Moreover, because phase separations of two different components often occur, binary mixed Langmuir monolayers and LB films that contain at least one low-molecular-weight component have also been widely studied.^{22–33} However, up to now, less work has been done on this subject with binary polymer mixtures because of their higher complexity.^{34–44}

It is known that homopolystyrene (h-PS) usually does not easily form a uniform and stable monolayer at the air/water interface because of the lack of hydrophilic groups.^{38,45} However, our recent work³⁴ shows there exists a composition window (about 80–95 wt % h-PS) for mixed Langmuir monolayers of h-PS and a symmetric diblock copolymer polystyrene-*block*-poly(2-vinylpyridine) (PS-*b*-P2VP) to form highly uniform and dense necklace-network structures in which PS nanoaggregates are in contact with each other. Our necklace networks are quite different from the dense nanostrand networks,²⁶ relatively loose networks,³⁸ and dense nanowire networks.⁴¹ In order to study further the possible mechanism and control the network structures (i.e., surface coverage and nanoaggregate diameter), the effects of spreading solution concentration and volume, subphase temperature, and transfer pressure on the mixed Langmuir monolayers and LB films of h-PS (90%) and the symmetric PS-*b*-P2VP (10%) were studied by means of the Langmuir monolayer technique and tapping mode atomic force microscopy (AFM), respectively.

* To whom correspondence should be addressed. Phone: +86 451 8639-2590. Fax: +86 451 8639-2577. E-mail: gywen@hrbust.edu.cn.

TABLE 1: Spreading Conditions of the Samples

spreading condition	I	II	III	IV	V
<i>c</i> (mg/mL)	0.50	0.50	0.50	0.75	1.00
<i>V</i> (μ L)	200	400	500	333	250
<i>A</i> _{ini} ^a (\AA^2)	297	148	119	119	119

^a *A*_{ini} means the initial area per 2VP unit after the spreading of a solution.

Experimental Section

Materials. Polymer materials of h-PS (PS15K, *M*_w = 15 000, *M*_w/*M*_n = 1.03) and a symmetric diblock copolymer PS-*b*-P2VP (SVP56K, *M*_n(PS) = *M*_n(P2VP) = 28 000, *M*_w/*M*_n = 1.05) used in this work were previously synthesized by anionic and sequential anionic polymerizations, respectively.

Preparation of the Spreading Solutions. The common solvent chloroform (CHCl₃, HPLC grade, Mallinckrodt) was used to prepare the stock solutions of PS15K and SVP56K with different concentrations of 0.50, 0.75, and 1.00 mg/mL. The spreading solutions of a mixture of PS15K and SVP56K (9:1, w/w, coded as PS15K-90%) with different concentrations were prepared by mixing the corresponding stock solutions in a volume ratio of 9:1. The spreading solutions were stored in a refrigerator and used within a week to avoid the concentration change.

π -A Experiments. Surface pressure–unit area (π -A) isotherms of PS15K-90% under different spreading conditions were characterized with a Langmuir film balance apparatus (KSV5000, Finland). The *M*_n of the mixture was used, for the LB software, to calculate the mean molecular area which was transformed further into area per 2VP unit during the drawing of the isotherms with the Origin software. The spreading conditions I–V with different concentrations (*c*) and volumes (*V*) of the samples are listed in Table 1. According to the experiment design, spreading conditions I–III were with the same concentration of 0.50 mg/mL and different volumes and spreading conditions III–V were with different concentrations and different volumes but with the same polymer amount. The

TABLE 2: Areas per 2VP Unit (\AA^2) under Different Transfer Pressures (π_t) and Different Spreading Conditions at 25 °C

π_t (mN/m)	I	II	III	IV	V
0.5	142	111	97	82	63
2	104	91	83	65	52
10	72	66	62	49	42

initial surface pressures of the mixed monolayers spread at 25 °C were usually about or below 0.1 mN/m. As for the KSV5000 apparatus, the effective areas of the two troughs were both about $705 \times 120 \text{ mm}^2$ and the platinum Wilhelmy plates were used as the surface pressure sensors. The subphase water (resistivity of $18 \text{ M}\Omega\cdot\text{cm}$) used for the isothermal experiments was purified and deionized with a water purification system (Pure Power II, Human, Korea) equipped with an organic removal cartridge. The spreading solutions were carefully dropped here and there (as uniformly as possible) with some evaporation in between onto the water surface with a gastight Hamilton mini-syringe. A 20 min period was allowed for the evaporation of CHCl_3 before the compression was initiated. Most of the measurements were performed at 25 °C (except for the temperature effect experiments) by using a refrigerated bath circulator (RBC-10, Jeio Tech, Korea). The Langmuir monolayers were compressed symmetrically with two barriers whose relative moving speed was 10 mm/min. All of the isotherms were run for several times, and at least two or three curves were superposed to make sure of good reproducibility.

Preparation of the LB Films. The KSV5000 apparatus was also used to transfer the Langmuir monolayers onto the silicon wafers, and thus, the corresponding LB films under different surface pressures, mainly 0.5, 2, and 10 mN/m, were obtained. Prior to the transfer, the silicon wafers were treated to be hydrophilic according to the following procedure and the silicon wafers were rinsed thoroughly with deionized water after each step: ultrasonic cleaned separately in chloroform and in a mixture of deionized water and 2-propanol (2:1 in volume) at room temperature for 10 min, treated in a mixture of deionized water, ammonia–water, and hydroperoxide (5:1:1 in volume) at 80 °C for 10 min, treated in a mixture of deionized water, hydrochloric acid, and hydroperoxide (6:1:1 in volume) at 80 °C for 15 min, treated in deionized water at 80 °C for 15 min, and finally blow-dried with ultrapure nitrogen. According to the isotherms shown later, the areas per 2VP unit (\AA^2) under different transfer pressures (π_t) and different spreading conditions are listed in Table 2. To obtain a stable monolayer, the surface pressure was maintained for 20 min before a transfer. During the transfer, the substrate was withdrawn vertically through the monolayer at a speed of 3 mm/min.

AFM Measurements. The LB films were characterized with a tapping mode AFM (Nanoscope IIIa, Digital Instruments) at room temperature. The $10 \mu\text{m}$ scanner and the etched silicon probes with resonant frequencies of 200–400 kHz and spring constants of 20–100 N/m were used. The scan areas and speeds of the AFM measurements were usually $2 \mu\text{m} \times 2 \mu\text{m}$ and about 0.8–1.0 Hz, respectively. Usually, two or three LB films were obtained and scanned for each condition. For an LB film, the AFM images were usually taken three to four times at different places, far from the edges, to make sure of good reproducibility. Most of the AFM height images ($1 \mu\text{m} \times 1 \mu\text{m}$) shown here were zoomed from the large ones.

Results and Discussion

Effect of Spreading Conditions on the Isotherms. The surface pressure–area per 2VP unit (π – A) isotherms of PS15K-

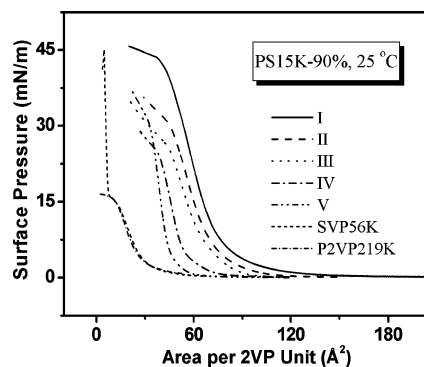


Figure 1. π – A isotherms of PS15K-90% monolayers spread with conditions I–V at 25 °C. For comparison, the isotherms of pure SVP56K and pure P2VP219K monolayers are also shown.

TABLE 3: Limiting Areas (A_0), Compressibility Values (C_m), and Collapse Pressures (π_c) Obtained from Figure 1

isotherm	I	II	III	IV	V	SVP56K
$A_0 (\text{\AA}^2)$	77	74	70	56	45	8
$C_m (\times 10^{-3} \text{ m/mN})$	16	17	19	24	15	14
$\pi_c (\text{mN/m})$	44	30	26	24	30	45

90% monolayers spread with conditions I–V at 25 °C shown in Figure 1 were characterized by the Langmuir monolayer technique. For comparison, Figure 1 also shows the isotherms of pure SVP56K and pure P2VP219K, which superpose well until the end of the quasi-plateau. From Figure 1, it can be seen that the isotherms of the mixed monolayers are featureless and the surface pressures increase steeply, which completely eliminates the quasi-plateau character of P2VP at intermediate surface concentration, and the isotherms of spreading conditions I–V shift to the small areas. Table 3 lists the limiting areas per 2VP unit (A_0), the monolayer compressibility (C_m), and the collapse pressures (π_c) for all of the samples obtained from Figure 1. The limiting areas describing the chain packing density within the densely packed aggregates were determined by extrapolating the steep linear region to the surface pressure of zero. According to ref 12a, the monolayer compressibility values were determined using $C_m = -1/A_0(\partial A/\partial \pi)_T$, where $(\partial A/\partial \pi)$ were taken at the inflection points of the π – A isotherms. With the increase of spreading volume and concentration, the limiting areas of the PS15K-90% monolayers decrease, which is easy to understand that the local chain packing density in the nanoaggregates increases with the evaporation of solvent, mainly due to chain entanglements during spreading. Furthermore, it can be seen that the effect of concentration on the isotherms is larger than that of volume, and thus the significant difference was mainly caused by a change in concentration for conditions III–V. The decrease effect of spreading concentration on the limiting area was also observed by Cheyne and Moffitt in the system of polystyrene-*b*-poly(ethylene oxide) (PS-*b*-PEO).¹² According to Table 3, the compressibility values increase and the collapse pressures decrease in a stepwise fashion except for condition V. It can be seen that the compressibility values are independent of the limiting areas. The monolayer of condition V is the most incompressible, which indicates that three-dimensional (3D) aggregates have already formed after spreading due to the high concentration. The A_0 and C_m in the pancake regions of SVP56K and P2VP219K are, respectively, evaluated as 30 and 27 \AA^2 and 50×10^{-3} and $51 \times 10^{-3} \text{ m/mN}$, which is comparable with the data of pure PEO ($27 \text{ \AA}^2/\text{monomer}$ and $48 \times 10^{-3} \text{ m/mN}$).^{12a}

Temperature Effect on the Isotherms. Figure 2 shows the temperature effect on the π – A isotherms of PS15K-90%

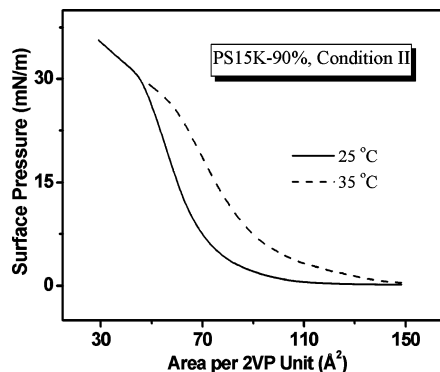


Figure 2. Temperature effect on the π -A isotherms of PS15K-90% monolayers spread with condition II.

monolayers spread with condition II. From Figure 2, it can be seen that the initial surface pressure, 0.4 mN/m, of the monolayer spread at 35 °C is significantly higher than that at 25 °C (about 0.1 mN/m), and the isotherm at 35 °C shifts to larger areas compared with that at 25 °C. The temperature effect on the isotherms of PS15K-90% is contrary to those of pure diblock copolymers SVP56K⁹ and PS₂₆₀-*b*-P4VP₂₄₀ quaternized with decyl iodide,²¹ which means the structures of the mixed Langmuir monolayers are quite different from those of the pure diblock copolymers with mainly isolated circular surface micelles. In this case, the elevation of temperature tends to improve the mobility of h-PS chains and thus increases the surface pressure. According to Figure 2, the areas per 2VP unit at 35 °C and under different transfer pressures, 0.5, 2, and 10 mN/m, are, respectively, 146, 122, and 84 Å².

AFM Images. In this part, the AFM height images of the LB films transferred under different pressures will be shown in the following figures in which the light regions represent the raised PS nanoaggregates. Figure 3 shows the AFM height images of the LB films of PS15K-90% from spreading conditions I–V transferred at 25 °C and under different pressures. According to Figure 3, the statistical information of the nanoaggregates, mainly the average diameter, surface coverage, and aggregation number of SVP56K, was evaluated by manual work and listed in Table 4. According to their diameter distribution, the nanoaggregates in a panel were classed into several kinds and counted, and the circular areas of the nanoaggregates were used to evaluate the average diameter. The total area of the nanoaggregates divided by the scan area was surface coverage. The aggregation number of SVP56K was calculated through dividing the area per aggregate by the area per P2VP block. Due to the quite large numbers counted by manual work, relative standard deviations in the number of aggregates, about ± 10 , were induced and resulted in the relative standard deviations of average diameter and surface coverage being, respectively, ± 1 and ± 3 . The relative standard deviations of aggregation numbers were usually about ± 0.1 to ± 0.3 and therefore not given in Table 4 except ± 4 in Vc.

From the AFM images of the LB films transferred under the relatively low pressure of 0.5 mN/m (a), it can be seen that a small volume effect (at the same concentration) exists on the average diameter (28, 30, and 31 nm) but a little larger effect exists on the surface coverage (24, 35, and 30%) for panels Ia, IIa, and IIIa. Furthermore, the nanoaggregates in the necklace-network structures (Ia and IIa) are with narrow diameter distributions when the spreading concentration and volume are both small, although a small amount of large ones due to the inactivity of the h-PS chains on the water surface exists. However, when the spreading concentration is a little higher

(IVa and Va), the surface coverages (43 and 49%) and the average diameters (32 and 37 nm) of the nanoaggregates are both a little larger compared with those of the other spreading conditions. With the increase of transfer pressure, the surface coverage usually tends to increase except for Ic and Vb (maybe due to the rather large change of the average diameter). The average diameter tends first to increase in Ib (39 nm), IIb (35 nm), and IVb (36 nm), which is expected due to the coalescence of some adjoining nanoaggregates, and then to decrease and obtain narrow distributions in Ic (24 nm), IIc (33 nm), and IVc (32 nm), which results from the split of large nanoaggregates into small ones. Furthermore, the average diameter tends to decrease in IIIb (23 nm) and Vb (32 nm) due to the split of large nanoaggregates, and then to increase in IIIc (31 nm) and Vc (83 nm) due to the coalescence of the adjoining nanoaggregates. At the air/water interface, the chain motion is possible to occur due to the high humidity and large amount of water molecules existing among the h-PS chains, which is likely to reduce the interaction between the h-PS chains. I believe the mobility of the chains on the water surface must be larger than those in LB films and those in the bulk. Furthermore, the barriers were moved back and forth for 20 min to maintain the surface pressure before a transfer, which would provide the necessary power for the chain motion. According to the above discussion, it is also possible to explain the aggregate diameter increase with the increase of transfer pressure for diblock copolymers PS-*b*-P2VP in my previous work,⁹ which cannot be explained with the assumption that the PS aggregates become kinetically frozen by vitrification upon solvent evaporation for the system of PS-*b*-PEO.¹²

It is worth noting that the shapes of some nanoaggregates are not completely circular and appear to be elongated in the perpendicular direction of the barrier compression especially when there are many large aggregates, e.g., IIIa, IIIc, and Vc. Moreover, the Z ranges of the AFM images are usually set as 15 nm except for the diameter decrease cases (about 10 nm in Ic, IIb, and IVc) and the cases Va (20 nm) and Vc (35 nm) with more and larger aggregates. It further indicates that 3D aggregates have already formed after spreading due to the high concentration, and Vc can be regarded as the eventual 3D aggregation morphology. At the moment, it is not clear whether aggregates have formed in the spreading solution at high concentration, especially for 1.00 mg/mL, which remains to be answered in future work. From Figure 3, it can be seen that spreading condition II with appropriate concentration and volume tends to form relatively uniform structures and spreading condition V with relatively high concentration tends to form large aggregates. According to Table 4, the aggregation numbers of SVP56K (between 5 and 13 under conditions I–IV) are far smaller than those of pure SVP56K (about 74 at 2 mN/m).^{9,10} With the increase of transfer pressure, for condition V, the aggregation numbers of SVP56K are, respectively, about 14, 13, and 89 which is even larger than that of pure SVP56K (86 at 7.5 mN/m)⁹ and is more evidence for the 3D aggregation morphology in Vc. It is worth noting that the varying trends of the aggregation numbers are totally consistent with those of the average diameters in all of the spreading conditions.

The AFM height images of the mixed LB films of PS15K-90% from spreading condition II transferred at 35 °C and under different pressures are shown in Figure 4. In the same way, the statistical information of the nanoaggregates in Figure 4 is listed in Table 5. With the increase of transfer pressure, it can be seen that the surface coverage increases step by step (34 to 47 to 91%) and the average diameter of the nanoaggregates first increases and then decreases

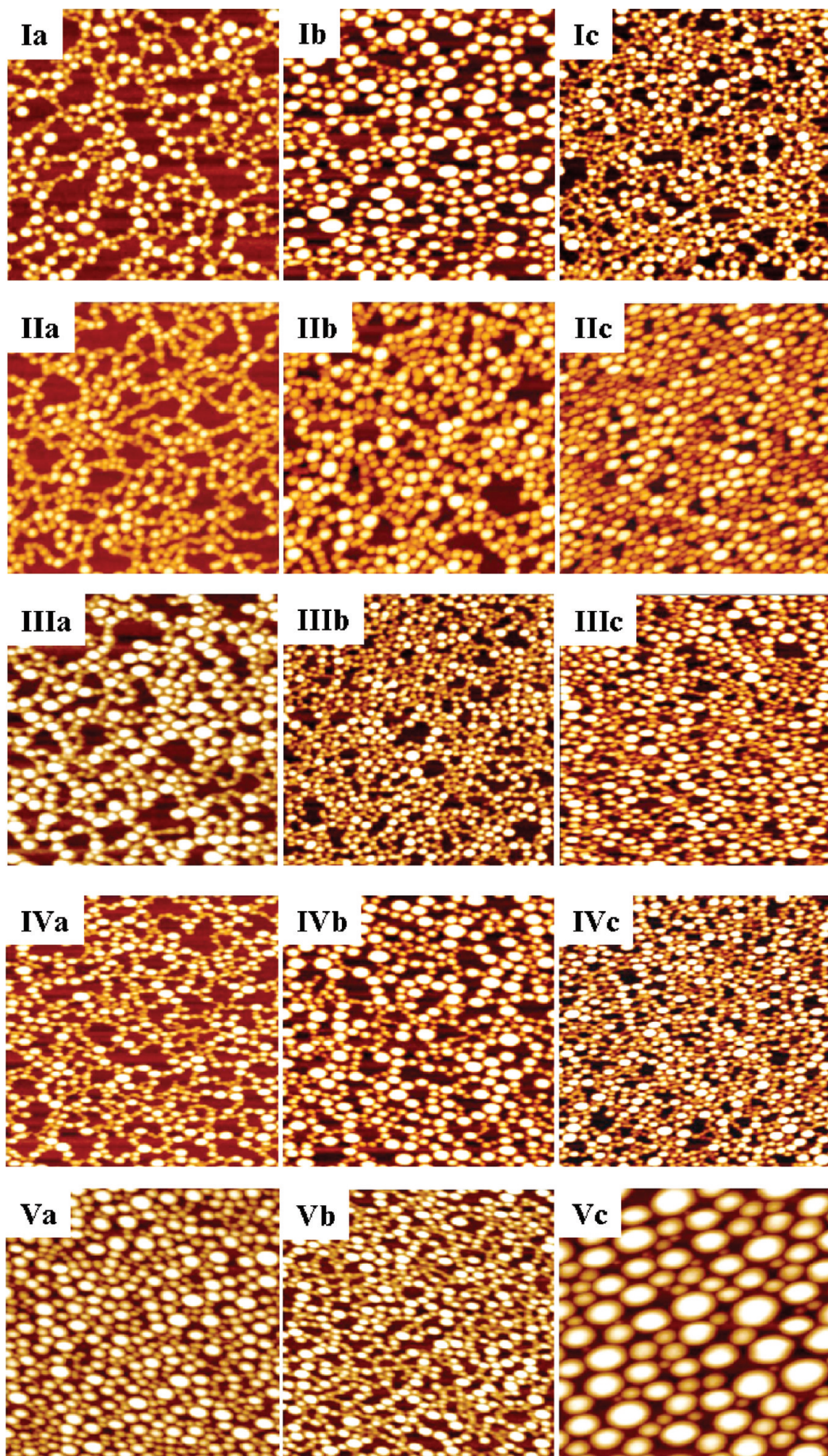


Figure 3. AFM height images ($1 \mu\text{m} \times 1 \mu\text{m}$) of the LB films of PS15K-90% from spreading conditions I–V transferred at 25 °C and under pressures of 0.5 (a), 2 (b), and 10 mN/m (c), respectively.

TABLE 4: Statistical Information of the Nanoaggregates in Figure 3^a

panel	Ia	Ib	Ic	IIa	IIb	IIc	IIIa	IIIb
number per μm^2	390 ± 10	340 ± 10	600 ± 10	500 ± 10	410 ± 10	570 ± 10	395 ± 10	830 ± 10
diameter range (nm)	20–60	20–80	20–60	20–40	30–60	30–60	20–60	20–40
average diameter (nm)	28 ± 1	39 ± 1	24 ± 1	30 ± 1	35 ± 1	33 ± 1	31 ± 1	23 ± 1
surface coverage (%)	24 ± 3	40 ± 3	27 ± 3	35 ± 3	39 ± 3	49 ± 3	30 ± 3	34 ± 3
N_{agg} of SVP56K ^b	7	11	9	7	10	10	10	6
Z range (nm)	15	15	10	12	15	15	15	10

panel	IIIc	IVa	IVb	IVc	Va	Vb	Vc
number per μm^2	575 ± 10	545 ± 10	450 ± 10	660 ± 10	440 ± 10	560 ± 10	100 ± 5
diameter range (nm)	20–60	30–40	20–60	30–40	30–60	30–40	30–140
average diameter (nm)	31 ± 1	32 ± 1	36 ± 1	32 ± 1	37 ± 1	32 ± 1	83 ± 1
surface coverage (%)	42 ± 3	43 ± 3	46 ± 3	52 ± 3	49 ± 3	45 ± 3	55 ± 3
N_{agg} of SVP56K	11	9	13	12	14	13	89 ± 4
Z range (nm)	15	15	15	10	20	15	35

^a Relative standard deviations obtained from the analysis of the AFM images for several times. ^b N_{agg} represents the aggregation number.

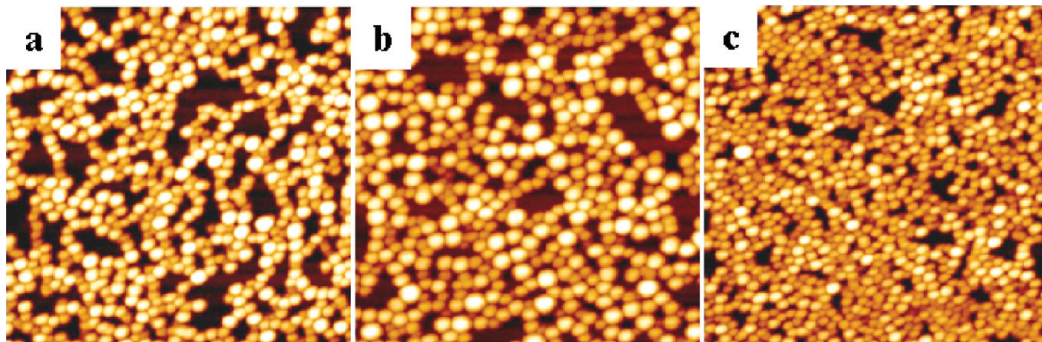


Figure 4. AFM height images ($1 \mu\text{m} \times 1 \mu\text{m}$) of the LB films of PS15K-90% from spreading condition II transferred at 35°C and under pressures of 0.5 (a), 2 (b), and 10 mN/m (c), respectively.

TABLE 5: Statistical Information of the Nanoaggregates in Figure 4

panel	a	b	c
number per μm^2	485 ± 10	350 ± 10	1285 ± 10
diameter range (nm)	20–40	40–50	20–40
average diameter (nm)	30 ± 1	41 ± 1	30 ± 1
surface coverage (%)	34 ± 3	47 ± 3	91 ± 3
N_{agg} of SVP56K	5	9	4
Z range (nm)	10	15	10

(30 to 41 to 30 nm). Compared with the LB films transferred at 25°C (in Figure 3, IIa–IIc), the diameter distribution in Figure 4 is a little narrower according to their diameter ranges. With the increase of transfer pressure, in Table 5, the aggregation numbers of SVP56K at 35°C are, respectively, smaller than those at 25°C . The Z ranges (10 nm) in Figure 4a and c are also smaller than those in Figure 3, IIa (12 nm) and IIc (15 nm). That is to say, the relatively higher humidity at 35°C is more beneficial for improving the mobility of the h-PS chains and results in the more uniform nanoaggregates.

Possible Mechanism. In order to further study the possible mechanism, I transferred an LB film under the initial pressure almost without compression. Figure 5 shows the AFM height images of the LB film of PS15K-90% from spreading condition II transferred at 25°C and under a pressure of less than 0.1 mN/m. From Figure 5, it can be seen that the uniform necklace-network structure has already formed before compression; that is, the network structure appeared to form spontaneously, which is different from those compression-induced network-like structures.^{25,26,38,41} The average diameter (24 nm), surface coverage (18%), and aggregation number of SVP56K (6) of the nanoaggregates in Figure 5b were also evaluated by manual work.

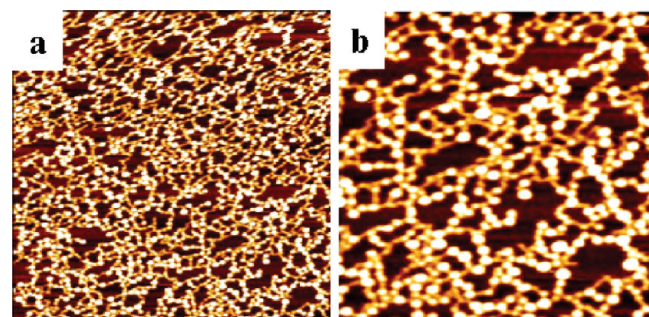


Figure 5. AFM height images of an LB film of PS15K-90% from spreading condition II transferred at 25°C and under a pressure of less than 0.1 mN/m. The areas of the images are, respectively, $2 \mu\text{m} \times 2 \mu\text{m}$ (a) and $1 \mu\text{m} \times 1 \mu\text{m}$ (b).

A possible mechanism for the aggregation behavior of the mixed monolayer of h-PS and PS-*b*-P2VP must contain their respective interface behavior and their synergetic effect. Dewetting of ultrathin films of homopolymers⁴⁶ and block copolymers^{12b,47} from solid and liquid surfaces is a common phenomenon. In the early 1990s, Reiter characterized the dewetting progression of PS, an extremely good model system, by annealing the films above the glass transition temperature (T_g). First, the films break up and appear as randomly distributed holes. Second, the holes grow and form polygon patterns of interconnected ribbons. Third, the resulting ribbons finally break down into droplets related to Rayleigh instabilities.⁴⁶ Cheyne and Moffitt presented the dewetting mechanism for the formation of PS-*b*-PEO aggregates at the air/water interface.^{12b} In my opinion, it seems that the dewetting of h-PS from the water surface is easier than that from the solid surface, and the later case usually occurs through annealing above T_g or solvent

treating for a relatively long time. Therefore, in this work, the dewetting of h-PS at the air/water interface is most likely to occur during the solution spreading and solvent evaporation, and finally forms the h-PS droplets.

On the other hand, a relatively low content of PS-*b*-P2VP (10%) and with an even lower content of the P2VP blocks (5%) tended to form a network of small micelles at the air/water interface. The quite small amount of P2VP blocks is not enough to cover the whole water surface, which can be concluded according to the facts that no significant contribution of P2VP blocks to the surface pressure can be found in the isotherms and the aggregation numbers of SVP56K in the mixed monolayers are far smaller than those of pure SVP56K. However, they tended still to spread out on the water surface and formed a network of small copolymer micelles. The synergetic effect, the h-PS droplets coalesce with the cores of the copolymer micelles, finally resulted in the formation of the relatively stable necklace-network structures.

Conclusions

Our recent work showed that a composition window existed for the mixed Langmuir monolayers of h-PS and the symmetric PS-*b*-P2VP to form the necklace-network structures at the air/water interface. In this work, the effects of spreading condition and transfer pressure on the Langmuir monolayers and the LB films of PS15K-90% were studied in detail. According to the results, it was possible to control the network structures (i.e., surface coverage and nanoaggregate diameter) by adjusting the spreading conditions and the transfer pressures. The spreading solutions with appropriate concentration and volume tended to form relatively uniform structures (e.g., condition II). With the increase of transfer pressure, there existed a novel nonlinear behavior for the nanoaggregate diameter first to increase, then to decrease, and finally to increase again, while the surface coverage tended to increase step by step. With the elevation of temperature, the chain motion between the adjoining nanoaggregates tended to be improved and thus the nanoaggregate diameter tended to be more uniform. A possible mechanism for the aggregation behavior of the mixed monolayer of h-PS and PS-*b*-P2VP is presented, which contains the formation of h-PS droplets via dewetting, network formation of small PS-*b*-P2VP micelles, and the synergetic effect of the h-PS droplets and the cores of the copolymer micelles. I think the uniform and stable necklace-network structures can be of some practical applications such as nanoelectronics and nanotemplate.

Acknowledgment. This work was supported by the National Natural Science Foundation of China (No. 20874024), the SRF for ROCS (State Education Ministry), the Scientific Research Fund of Heilongjiang Provincial Education Department (No. 11521042), and the Training Project for Outstanding Young Fellow of Harbin University of Science and Technology.

References and Notes

- (1) Roberts, G. G. *Langmuir-Blodgett Films*; Plenum Press: New York, 1990.
- (2) Ulman, A. *An Introduction to Ultrathin Organic Films -from Langmuir-Blodgett Films to Self-Assembly*; Academic Press: San Diego, CA, 1991.
- (3) Petty, M. C. In *Polymer Surface and Interface*; Feast, W. J., Munro, H. S., Eds.; John Wiley & Sons Ltd: Chichester, U.K., 1987; p 163.
- (4) Ogi, T.; Ohkita, H.; Ito, S.; Yamamoto, M. *Thin Solid Films* **2002**, 415, 228.
- (5) Deschenes, L.; Bousmina, M.; Ritcey, A. M. *Langmuir* **2008**, 24, 3699.
- (6) Joncheray, T. J.; Denoncourt, K. M.; Meier, M. A. R.; Schubert, U. S.; Duran, R. S. *Langmuir* **2007**, 23, 2423.
- (7) Peetla, C.; Graf, K.; Kressler, J. *Colloid Polym. Sci.* **2006**, 285, 27.
- (8) Zhang, J.; Cao, H.; Wan, X.; Zhou, Q. *Langmuir* **2006**, 22, 6587.
- (9) Wen, G.; Chung, B.; Chang, T. *Polymer* **2006**, 47, 8575.
- (10) Choi, M.; Chung, B.; Chun, B.; Chang, T. *Macromol. Res.* **2004**, 12, 127.
- (11) Ferreira, M.; Constantino, C. J. L.; Olivati, C. A.; Balogh, D. T.; Aroca, R. F.; Faria, R. M.; Oliveira, J. O. N. *Polymer* **2005**, 46, 5140.
- (12) (a) Cheyne, R. B.; Moffitt, M. G. *Langmuir* **2005**, 21, 5453. (b) Cheyne, R. B.; Moffitt, M. G. *Langmuir* **2006**, 22, 8387.
- (13) Kumaki, J.; Hashimoto, T. *J. Am. Chem. Soc.* **2003**, 125, 4907.
- (14) Ahmed, F.; Hategan, A.; Discher, D. E.; Discher, B. M. *Langmuir* **2003**, 19, 6505.
- (15) Fahmi, A. W.; Oertel, U.; Steinert, V.; Froeck, C.; Stamm, M. *Macromol. Rapid Commun.* **2003**, 24, 625.
- (16) Devereaux, C. A.; Baker, S. M. *Macromolecules* **2002**, 35, 1921.
- (17) Meli, M. V.; Badia, A.; Grüter, P.; Lennox, R. B. *Nano Lett.* **2002**, 2, 131.
- (18) Cox, J. K.; Yu, K.; Constantine, B.; Eisenberg, A.; Lennox, R. B. *Langmuir* **1999**, 15, 7714.
- (19) Lin, B.; Rice, S. A.; Weitz, D. A. *J. Chem. Phys.* **1993**, 99, 8308.
- (20) Zhu, J.; Lennox, R. B.; Eisenberg, A. *J. Phys. Chem.* **1992**, 96, 4727.
- (21) Zhu, J.; Eisenberg, A.; Lennox, R. B. *J. Am. Chem. Soc.* **1991**, 113, 5583.
- (22) Xu, M.; Sun, L.; Yin, S.; Liu, C.; Wu, L. *J. Colloid Interface Sci.* **2007**, 316, 912.
- (23) Hussain, S. A.; Paul, P. K.; Bhattacharjee, D. *J. Phys. Chem. Solids* **2006**, 67, 2542.
- (24) Mitamura, K.; Imae, T.; Mouri, E.; Torikai, N.; Matsuoka, H.; Nakamura, T. *J. Nanosci. Nanotechnol.* **2006**, 6, 36.
- (25) Hottle, J. R.; Deng, J.; Kim, H.-J.; Farmer-Creely, C. E.; Viers, B. D.; Esker, A. R. *Langmuir* **2005**, 21, 2250.
- (26) Lu, Q.; Bazuin, C. G. *Nano Lett.* **2005**, 5, 1309.
- (27) Matsumoto, M.; Tanaka, K.; Azumi, R.; Kondo, Y.; Yoshino, N. *Langmuir* **2003**, 19, 2802.
- (28) Dos Santos, D. S.; Mendonca, C. R.; Balogh, D. T.; Dhanabalan, A.; Giacometti, J. A.; Zilio, S. C.; Oliveira, O. N. *Polymer* **2002**, 43, 4385.
- (29) Silva, J. R.; Dall'Agnol, F. F.; Oliveira, O. N.; Giacometti, J. A. *Polymer* **2002**, 43, 3753.
- (30) Iimura, K.; Shiraku, T.; Kato, T. *Langmuir* **2002**, 18, 10183.
- (31) Liu, Y.; Liu, M. *Thin Solid Films* **2002**, 415, 248.
- (32) Simões Gamboa, A. L.; Filipe, E. J. M.; Brogueira, P. *Nano Lett.* **2002**, 2, 1083.
- (33) Fang, J.; Knobler, M. C. *Langmuir* **1996**, 12, 1368.
- (34) Wen, G.; Chung, B.; Chang, T. *Macromol. Rapid Commun.* **2008**, 29, 1248.
- (35) Price, E. W.; Guo, Y.; Wang, C.-W.; Moffitt, M. G. *Langmuir* **2009**, 25, 6398.
- (36) Chung, B.; Choi, H.; Park, H.-W.; Ree, M.; Jung, J. C.; Zin, W. C.; Chang, T. *Macromolecules* **2008**, 41, 1760.
- (37) Lopes, S. I. C.; Goncalves da Silva, A. M. P. S.; Brogueira, P.; Picarra, S.; Martinho, J. M. G. *Langmuir* **2007**, 23, 9310.
- (38) Li, B.; Esker, A. R. *Langmuir* **2007**, 23, 574.
- (39) Liu, J.; Zhang, Y.; Zhang, J.; Shen, D.; Guo, Q.; Takahashi, I.; Yan, S. *J. Phys. Chem. C* **2007**, 111, 6488.
- (40) Bosker, W. T. E.; Iakovlev, P. A.; Norde, W.; Cohen Stuart, M. A. *J. Colloid Interface Sci.* **2005**, 286, 496.
- (41) Seo, Y. S.; Kim, K. S.; Galambos, A.; Lammertink, R. G. H.; Vancso, G. J.; Sokolov, J.; Rafailovich, M. *Nano Lett.* **2004**, 4, 483.
- (42) Klass, J. M.; Lennox, R. B.; Brown, G. R. *Langmuir* **2003**, 19, 333.
- (43) Malzert, A.; Boury, F.; Saulnier, P.; Benoit, J. P.; Proust, J. E. *Langmuir* **2000**, 16, 1861.
- (44) Yamamoto, S.; Tsujii, Y.; Fukuda, T. *Polymer* **2000**, 42, 2007.
- (45) (a) Kumaki, J. *J. Polym. Sci., Part B: Polym. Phys.* **1990**, 28, 105. (b) Kumaki, J. *Macromolecules* **1988**, 21, 749. (c) Kumaki, J. *Macromolecules* **1986**, 19, 2258.
- (46) (a) Reiter, G. *Phys. Rev. Lett.* **1992**, 68, 75. (b) Reiter, G. *Langmuir* **1993**, 9, 1344.
- (47) (a) Green, P. F. *J. Polym. Sci., Part B: Polym. Phys.* **2003**, 41, 2219. (b) Limary, R.; Green, P. F. *Macromolecules* **1999**, 32, 8167. (c) Limary, R.; Green, P. F. *Langmuir* **1999**, 15, 5617.